Hindawi
Journal of Robotics
Volume 2022, Article ID 7164008, 9 pages
https://doi.org/10.1155/2022/7164008

Research Article

Coordinated Control of ESP-SAS System Considering Roll

Peng Wang,[1] **Yuan Ge**,[1] **Shanggui Cao**,[2] **Chao Han**,[1] **Ping Yang**,[1] **and Zhichao Zhang**[1]

[1]*School of Electrical Engineering, Anhui Polytechnic University, Wuhu 241000, China*
[2]*Chery Automobile Co., Ltd, Wuhu 241000, China*

Correspondence should be addressed to Yuan Ge; geyuan@ahpu.edu.cn

Received 28 September 2022; Revised 7 December 2022; Accepted 16 December 2022; Published 28 December 2022

Academic Editor: Ramadoni Syahputra

To improve the antiroll ability of the vehicle, considering the coupling characteristics of vehicle dynamics and tire force, this paper proposes a vehicle active antiroll strategy based on an electronic stability program and semiactive suspension (ESP-SAS) coordinated control. According to the motion characteristics of the electronic stability program (ESP) and semiactive suspension (SAS), the fuzzy controller based on the ESP module and the proportion integration differentiation (PID) controller based on the SAS module are designed, respectively. Through the adjustment of ESP yaw moment and the timely matching of SAS damping force, the antiroll performance of the vehicle is optimized. At the same time, due to the coupling characteristics between the two, a coordinated controller is designed to minimize the transfer of tire dynamic load. The proposed strategy is simulated and verified by Fishhook test conditions. As is shown from the results, with a good effect on the control of vehicle roll risk, the proposed coordinated control strategy can not only effectively reduce the body roll angle but also improve the operation stability of the vehicle.

1. Introduction

As the development of society facilitates people's traveling demand, the consumption of the automobile market is on the rise, and the incidence of traffic accidents is rising accordingly, which puts a serious menace to people's life and property [1, 2]. A vehicle rollover is a common traffic accident. Although rollover accounts for a low proportion of the entire traffic accident, the probability of serious injury and death of the occupant in the accident is high. Therefore, it is necessary to further study the vehicle rollover problem [3–5].

In recent years, many scholars and automobile manufacturers at home and abroad have conducted extensive research to improve the antiroll ability of vehicles. References [6, 7] adopted the yaw-roll joint control model based on the Takagi–Sugeno (T-S) method and carried out the improved sliding mode control of active yaw moment and roll moment in the nonlinear working domain. This is to realize joint control of tilt motion from the yaw side of the cargo vehicle. References [8, 9] proposed an optimal robust control strategy using the linear matrix inequality method for coupling vehicle lateral, yaw, and roll dynamics to gain yaw and roll stability. The yaw stabilization and rollover prevention functions are realized with the active suspension system. A state feedback fuzzy distributed controller is designed by Reference [10], which focuses on the solution of vehicle steering nonlinearity and actuator saturation in the limit state. Experiments show that the control of the nonlinear steering process is more accurate, the actuator capability is more fully utilized, and the control stability is maintained under the input saturation constraint. Reference [11] proposed a force-driven model predictive control (MPC) path tracking control strategy based on the coordination of optimal front wheel lateral force and additional yaw moment. Reference [12] proposed a sliding mode control (SMC) method based on an adaptive radial basis function neural network (ARBF-NN) for vehicle headway and optimal speed tracking, which effectively adjusted the traffic disturbance during the whole road operation.

Reference [13] proposed a new control strategy. By modeling the longitudinal dynamics of the truck and the engine fuel consumption model, the expected engine torque or expected braking torque of the following vehicle is derived by using the dynamic equation, and the decision of the following vehicle on the throttle opening and wheel cylinder pressure according to the actual situation is realized.

In addition, the controller method with suspension or electronic stability system is used in the vehicle antiroll solution. Aiming to deal with the rollover of mini-buses during driving, references [14–16], respectively, established active suspension and differential braking antirollover control subsystems and proposed an integrated antirollover control strategy to reduce the vehicle yaw rate and body roll angle to achieve antirollover control. Reference [17] proposed a hierarchical stability control strategy. Through model predictive control (MPC), the vehicle stability was set as the optimization objective, and the motor limit torque was used as the constraint condition. Finally, the simulation results show that the proposed control strategy can improve the stability and safety of a four-wheel independent drive electric vehicle. A distributed cooperative control structure, as References [18–21] proposed, adjusts the roll dynamics by controlling the damping force of the semiactive suspension and suppresses the overshoot and oscillation of yaw rate and lateral velocity. References [22–24] designed a coordination strategy based on fuzzy logic to coordinate each subcontrol, including active steering, active braking, and active roll control systems. The results of the experiments indicate that the integrated controller can successfully restore the stability of the vehicle in critical conditions. References [25–27] utilized an electronic stability program and designed a fuzzy controller to control the instability of vehicles with the Active Antiroll Bar (AARB) and carried out simulation experiments. Not only can the integrated control effectively control the vehicle rollover and instability, but it can also effectively improve the yaw and roll stability of the vehicle.

Despite the considerable investigations conducted mentioned above, none of the scholars fully considered the coupling characteristics between the vehicle electronic stability program (ESP) module and semiactive suspension (SAS) module. Therefore, this paper proposes an ESP-SAS system based on coordinated control, which improves the roll stability of the vehicle through the adjustment of yaw moment and the real-time matching of suspension force. Specifically, the yaw moment and antiroll moment required for vehicle antiroll are generated by the ESP module and SAS module, respectively, and the coordinated controller is designed to deal with the torque loss caused by the simultaneous operation of the two systems. Finally, the roll risk of the vehicle is evaluated by calculating the lateral load transfer rate online.

With a sport utility vehicle (SUV) is taken as the research object, of which the parameters are shown in Table 1. Based on the in-depth investigation of vehicle roll stability, the coordinated control of ESP and SAS is studied. The introduction of this paper is arranged as follows. Section 1 establishes a three-degree-of-freedom rollover model of the vehicle and calculates the lateral load transfer rate of the vehicle. In Section 2, the controller of the ESP module and SAS module are introduced. In Section 3, the design of the coordinated controller is emphasized. In Section 4, the Fishhook test simulation is carried out in CarSim and Simulink and the results are discussed. Section 5 gives the conclusion of this paper.

Table 1: Vehicle parameters.

Vehicle parameters	Value	Unit
m_c	1341	kg
I_z	1536.7	$\mathrm{kg}\cdot\mathrm{m}^2$
l_f	1.015	m
l_r	1.895	m
k_f	23580	N/rad
k_r	21300	N/rad

2. Vehicle Dynamics Model and Load Transfer Ratio

2.1. Vehicle Dynamics Model. To investigate the vehicle roll stability, it is assumed that the road surface is flat and the road adhesion coefficient is known. At the same time, the vertical motion and pitch motion of the vehicle are ignored, and only the motion in the longitudinal, roll, and yaw directions are considered. According to the joint modeling method, a three-degree-of-freedom (3-DOF) dynamic model of the vehicle is obtained as shown in Figure 1.

The lateral motion equation and yaw motion equation shown in Figure 1(a) are as follows:

$$\begin{aligned} m\left(\dot{v}_y + v_x\omega_r\right) - m_s h_s\ddot{\varphi} &= \left(F_{\mathrm{yfl}} + F_{\mathrm{yfr}}\right)\cos\delta + \left(F_{\mathrm{yrl}} + F_{\mathrm{yrr}}\right), \\ I_z\dot{\omega}_r &= l_f\left(F_{\mathrm{yfl}} + F_{\mathrm{yfr}}\right)\cos\delta - l_r\left(F_{\mathrm{yrl}} + F_{\mathrm{yrr}}\right) + M_z, \end{aligned} \tag{1}$$

where m and m_s are the vehicle mass and sprung mass, respectively; v_x and v_y are the longitudinal velocity and lateral velocity of the vehicle, respectively; h and h_s are the height of the center of mass of the vehicle body and the height from the center of mass to the roll center, respectively; δ is the front wheel angle; φ is the roll angle of the vehicle; ω_r is the yaw rate of the vehicle body; I_z is the yaw moment of inertia; l_f, l_r are the front and rear wheelbases of the vehicle, respectively; $F_{yi}\,(i = fl, fr, rl, rr)$ is the lateral force of the left front wheel, the right front wheel, the left rear wheel and the right rear wheel of the vehicle, respectively; M_z is the additional yaw moment of the vehicle.

And, the roll motion equation shown in Figure 1(b) is as follows:

$$I_x\ddot{\varphi} - m_s h_s\left(\dot{v}_y + v_x\omega_r\right) = m_s g h_s\sin\varphi - k_\varphi\varphi - c_\varphi\dot{\varphi} + M_x, \tag{2}$$

where k_φ and c_φ are roll angle stiffness and roll angle damping, I_x is roll moment of inertia and M_x is vehicle antiroll moment.

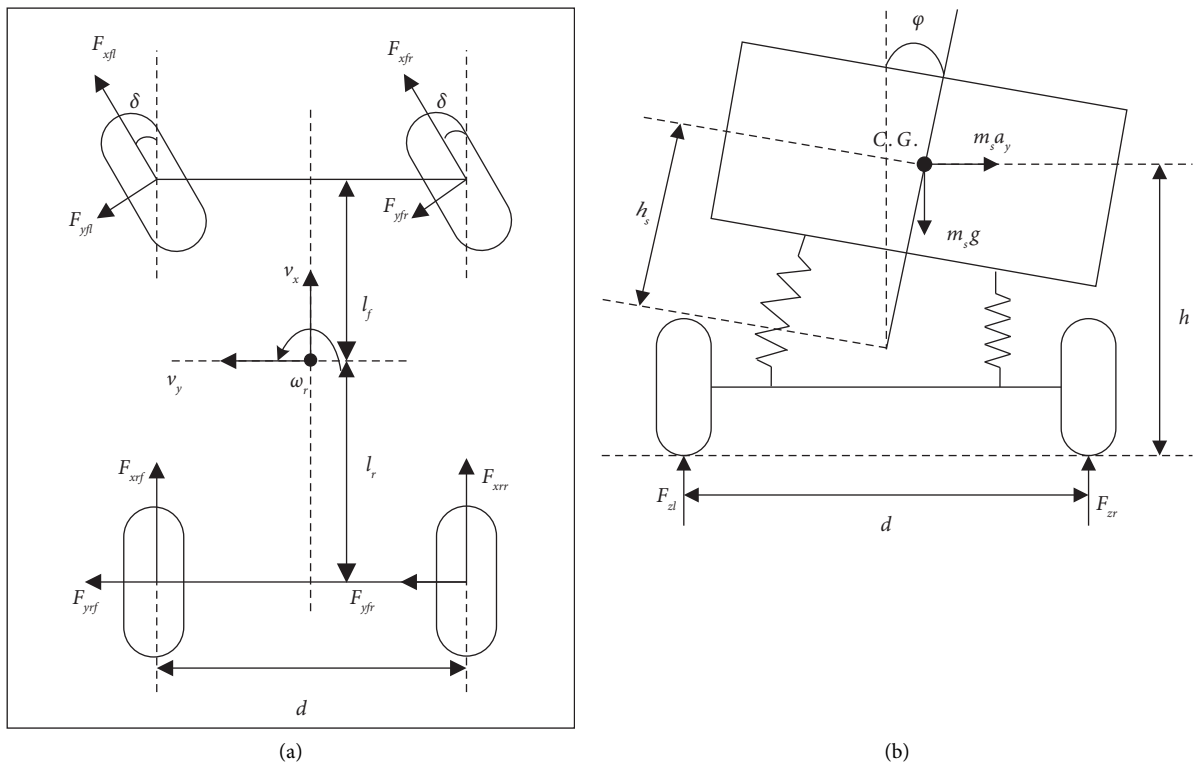

Figure 1: 3-DOFs vehicle dynamics model. (a) Lateral model. (b) Roll model.

2.2. Calculation of an LTR. Load Transfer Ratio (LTR) is the main evaluation index of vehicle roll stability, which can effectively describe the possibility of vehicle rollover. It is defined as the ratio of the difference between the vertical loads on the wheels on both sides of the vehicle to the sum of the vertical loads on both sides, which is as follows:

$$\mathrm{LTR} = \frac{F_{zl} + F_{zr}}{F_{zl} - F_{zr}}, \tag{3}$$

where F_{zl} and F_{zr} are the total tire loads on the left and right sides of the vehicle, respectively.

Because the vertical load on both sides of the tire is not easy to measure, according to the 3-DOF vehicle model established in 1.1, the LTR formula can be expressed as follows:

$$\mathrm{LTR} = \frac{2}{dm_s g}\left[m_s g h_s \varphi + m_s\left(\dot{v}_y + v_x \omega_r\right) - I_x \ddot{\varphi}\right]. \tag{4}$$

From the expression of LTR, the LTR value is a variable between 0 and 1. When LTR = 0, the vertical load of the left tire of the vehicle is equal to that of the right tire, indicating that the vehicle is driving stably at this time. When LTR = 1, the vertical load of the left tire or the right tire of the vehicle is 0, and one side of the wheel has completely left the ground, which will lead to a rollover accident will occur. Considering response time and vehicle system operation, the LTR threshold is 0.7.

3. Design of ESP and SAS Controllers

3.1. Establishment of 2-DOF Model. The ESP controller can improve the operating stability of the vehicle by controlling the deviation between the actual value and the expected value of the state variable. Owing to the simple structure of the two-degree-of-freedom model, the greatest impact on the lateral motion of the vehicle yaw rate and sideslip angle variables is taken into account. Hence, this paper uses the two-degree-of-freedom (2-DOF) model to calculate the expected value of the vehicle motion state control quantity. The differential equation is as follows:

$$\begin{cases} m\left(\dot{v}_y + v_x \omega_r\right) = \left(k_f + k_r\right)\beta + \dfrac{\omega_r}{v_x}\left(ak_f - bk_r\right) - k_f \delta, \\ I_z \dot{\omega}_r = \left(ak_f - bk_r\right)\beta + \dfrac{\omega_r}{v_x}\left(a^2 k_f - b^2 k_r\right) - ak_f \delta, \end{cases} \tag{5}$$

where k_f, k_r are equivalent cornering stiffness of the front and rear wheels, respectively.

Considering the actual situation of vehicle driving, the yaw rate and sideslip angle formula constraints are as follows:

$$\begin{cases} \omega_{r\max} = \dfrac{\mu g}{v_x}, \\ \beta_{\max} = \mu \cdot g\left(\dfrac{l_r}{v_x^2} + \dfrac{ml_f}{k_r L}\right), \end{cases} \tag{6}$$

where μ is the adhesion coefficient of the ground and g is the acceleration of the center of gravity, $L = l_f + l_r$.

Therefore, the value smaller than the absolute values of the two is taken as the expected value, and the expected values of the vehicle yaw rate and the sideslip angle are

$$\begin{cases} \omega_{rd} = \min\left\{\left|\omega_r\right|, \left|\omega_{r\max}\right|\right\}, \\ \beta_{rd} = \min\left\{\left|\beta\right|, \left|\beta_{\max}\right|\right\}. \end{cases} \tag{7}$$

3.2. Design of ESP Controllers. The vehicle ESP controller is designed to prevent the vehicle from entering an uncontrollably unstable state through active control of the critical driving state. In this paper, the method of the fuzzy controller is adopted. The difference between the expected value and the actual value of the yaw rate and the difference between the expected value and the actual value of the sideslip angle are taken as input, and the output is the additional yaw moment. Under a reasonable braking control strategy, the generated yaw moment is distributed to each wheel. The ESP controller design is demonstrated in Figure 2.

The language input and output variables of the designed fuzzy subset are divided into seven fuzzy levels:

$$\begin{aligned} \left\{E_\beta, E_\omega\right\} &= \{NB, NM, NS, ZO, PS, PM, PB\}, \\ \{\Delta M\} &= \{NB, NM, NS, ZO, PS, PM, PB\}. \end{aligned} \tag{8}$$

The basic domain range of the error is set to [−6, 6]. According to the actual situation of the input and output variables, the scale factor and the quantization factor are set, respectively. The fuzzy control rules are shown in Table 2.

To make full use of the tire braking force and to generate greater additional yaw moment, the additional yaw moment control strategy of unilateral two-wheel braking is adopted to quickly restore the vehicle from the unstable state to the stable state. The unilateral two-wheel braking strategy is to brake the left front wheel and the left rear wheel or the right front wheel and the right rear wheel simultaneously according to the insufficient steering or excessive steering of the vehicle.

3.3. Design of SAS Controller. Because the PID controller is easy to implement in structure and the parameters are easy to adjust, the PID controller has been widely used in engineering. Therefore, PID control is used as a SAS controller to calculate the antiroll torque. The ideal value of the body roll angle is set as $\varphi_{rd} = 0$, and the deviation between the ideal value and the actual value of the body roll angle is taken as the input of the PID controller. The controller block diagram is shown in Figure 3.

The digital PID formula can be expressed as

$$u(t) = K_p e(t) + K_I \int_0^t e(t)\mathrm{d}t + K_D \frac{de(t)}{dt}, \tag{9}$$

where K_p, K_I, K_D are, respectively, expressed as a proportional coefficient, integral coefficient, and differential coefficient.

The antiroll torque calculated by the PID controller needs to be realized by suspension force. When the vehicle rolls, the antiroll torque is distributed to the preset suspension module to achieve the vehicle antiroll effect. Take the front wheel corner left in a positive direction, the specific allocation scheme is shown in Table 3.

4. Establishment of a Coordinated Controller

4.1. Analysis of Tire Dynamic Load. When the ESP controller and the SAS controller work at the same time, the vertical load of each wheel will transfer to varying degrees. When the ESP controller works, the braking will change the vertical load of the front axle and the rear axle of the vehicle. At this time, the lateral force generated by the wheel deflection will affect the lateral acceleration and the yaw moment. When the SAS controller works, the vertical load on the left and right sides of the vehicle will change. The wheel with increased vertical load can provide greater longitudinal braking force, while the wheel with reduced vertical load can provide less maximum longitudinal braking force. Therefore, when ESP and SAS system work at the same time, the resulting yaw moment and roll torque will endure a part of the loss.

The dynamic analysis of the vehicle in roll state is carried out, and the vehicle tire dynamic load formula is established. The longitudinal dynamic load is shown as follows:

$$\begin{aligned} \Delta F_{\mathrm{zfl}} &= \Delta F_{\mathrm{zfr}} \\ &= \frac{\left(m_s a_x h_s + m_w h_f a_x + m_w h_r a_x\right)}{2\left(l_f + l_r\right)}, \\ \Delta F_{\mathrm{zrl}} &= \Delta F_{\mathrm{zrr}} \\ &= -\left(\frac{\left(m_s a_x h_s + m_w h_f a_x + m_w h_r a_x\right)}{2\left(l_f + l_r\right)}\right), \end{aligned} \tag{10}$$

where h_f, h_r is the height of the center of mass of the front and rear axles of the vehicle from the ground, and m_w is the mass of the vehicle tire.

The transverse dynamic load is shown as follows:

$$\begin{aligned} \Delta F_{zl} &= \frac{\left(\left(m_s a_y l_r h/d\right) - c_\varphi \varphi + m_s h_f a_y\right)}{d}, \\ \Delta F_{zr} &= \frac{\left(\left(m_s a_y l_r h/d\right) - c_\varphi \varphi + m_s h_r a_y\right)}{d}. \end{aligned} \tag{11}$$

According to (10) and (11), the dynamic vertical load is affected by longitudinal acceleration and lateral acceleration. In this paper, consequently, a coordinated controller based on longitudinal acceleration and lateral acceleration is designed, and the compensation torque generated by the coordinated controller is used to compensate for the loss of torque caused by the simultaneous operation of ESP and SAS systems. At this time, the total yaw moment and roll moment generated by the entire controller are expressed as

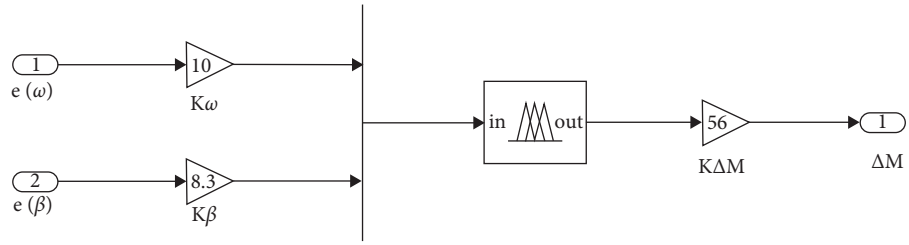

Figure 2: Diagram of the fuzzy controller.

Table 2: ESP fuzzy logical rules.

E_ω	E_β						
	NB	NM	NS	ZO	PS	PM	PB
NB	NS	NS	NS	NM	NB	NB	NB
NM	NS	NS	NS	NM	NM	NB	NB
NS	NS	NS	NS	NS	NM	NM	NB
ZO	PM	PM	PS	ZO	NS	NM	NM
PS	PB	PM	PM	PM	PS	PS	PS
PM	PB	PB	PM	PM	PS	PS	PS
PB	PB	PB	PB	PM	PS	PS	PS

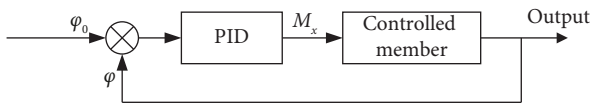

Figure 3: Diagram of the suspension controller.

Table 3: Antiroll torque distribution scheme.

δ	Roll trend	Suspension force distribution
$\delta > 0$	Right-side	Right wheel (50% each)
$\delta < 0$	Left-side	Left wheel (50% each)

$$\begin{aligned} M_{\text{zdes}} &= M_{\text{Fuzzy}} + M_{zc}, \\ M_{\text{xdes}} &= M_{\text{PID}} + M_{xc}, \end{aligned} \tag{12}$$

where $M_{\text{Fuzzy}}, M_{\text{PID}}$ is the yaw moment generated by the ESP controller and the roll moment generated by the SAS controller, and M_{zc}, M_{xc} is the yaw moment and roll moment generated by the coordinated controller.

The compensation controller designed according to the longitudinal acceleration and lateral acceleration is as follows:

$$\begin{aligned} M_{zc} &= k_1 a_x + k_2 a_y, \\ M_{xc} &= k_3 a_x + k_4 a_y, \end{aligned} \tag{13}$$

where k_1, k_2 are the longitudinal acceleration coefficient and lateral acceleration coefficient of the yaw moment of the coordinated controller, and k_3, k_4 are the longitudinal acceleration coefficient and lateral acceleration of the roll moment of the coordinated controller.

The system design diagram with the addition of the coordination controller is exhibited in Figure 4.

4.2. The Basic Principle of Particle Swarm Optimization Algorithm. The particle swarm optimization algorithm is an intelligent optimization algorithm proposed by Dr. Eberhart and Dr. Kennedy in 1995 based on the process of birds searching for food. The basic idea is to find the optimal solution through information sharing and collaboration between individuals in the group. The flow chart of the Particle Swarm Optimization Algorithm (PSO) algorithm is shown in Figure 5.

The PSO algorithm searches aim to find the feasible solution value of the region around the particle and calculates the fitness value after the fitness function is introduced. After comparison, the velocity and position in the particle iteration process are updated. In the process of solving, the particle swarm optimization algorithm will produce two optimal solutions, one is the optimal solution P_{best} found by the particle itself, and the other is the optimal solution G_{best} found by the group.

The velocity and position update equations for particles are as follows:

$$\begin{cases} v^{t+1} = w \cdot v^t + c_1 \cdot r_1\left(P_{\text{best}} - x^t\right) + c_2 \cdot r_2\left(G_{\text{best}} - x^t\right), \\ x^{t+1} = x^t + v^{t+1}. \end{cases} \tag{14}$$

To make the vehicle recover from the rollover as soon as possible and to avoid the vehicle instability caused by the excessive suspension displacement induced by the extreme distribution of vertical force, the objective function of PSO is constructed by minimizing the variance of the vertical force dynamic coefficient.

$$\min J = \left(\frac{1}{4}\sum_{i=1}^{4}\left(\varepsilon_i - \frac{1}{4}\sum_{i=1}^{4}\varepsilon_i\right)^2\right)^{1/2}, \tag{15}$$

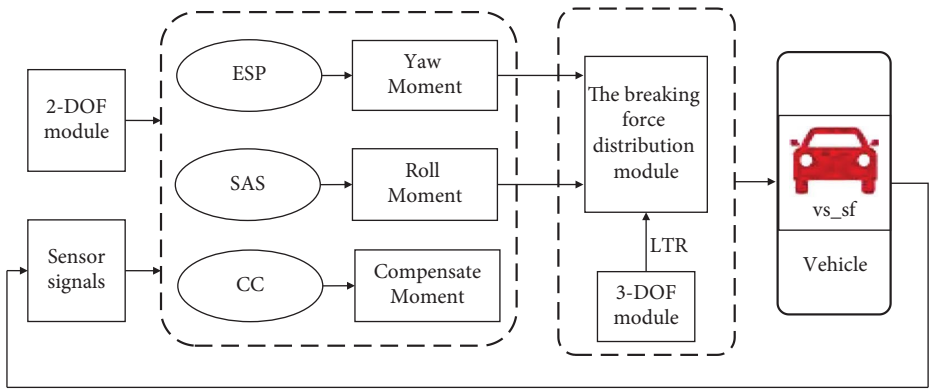

Figure 4: Block diagram of coordination controller.

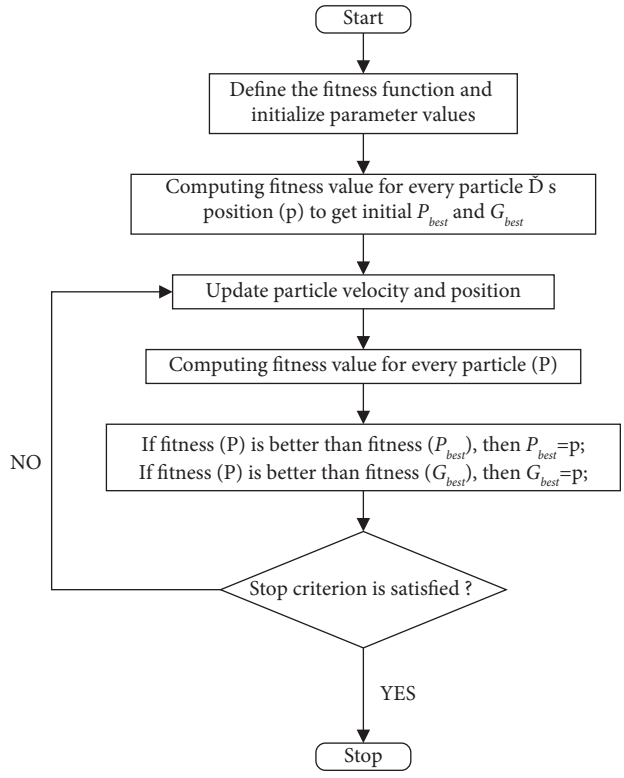

Figure 5: Flow chart of particle swarm algorithm.

where $\varepsilon_i = F_{zi,0}/F_{zi}$ is the dynamic coefficient of the vertical force of tire; $F_{zi,0}$ is the static load of each wheel when the vehicle stops completely on the horizontal ground; F_{zi} is the dynamic load of vehicle.

5. Simulation and Result Analysis

To verify the effectiveness of the proposed coordinated controller, the vehicle model and control module are established based on Carsim and Simulink, respectively. Through the joint simulation of Carsim and Simulink, the simulation and result analysis are both carried out in the Fishhook test. The vehicle model parameters taken are shown in Table 1.

The schematic diagram of the Fishhook test condition is shown in Figure 6. The vehicle steering wheel first turns left 270 deg and then turns right 540 deg and the vehicle operation is observed. Among them, The road adhesion coefficient $\mu = 0.85$ of the test condition and the initial vehicle speed $v_x = 80$ km/h.

To observe the effect of the controller, this paper runs the ESP controller alone (ESP-Only), the ESP controller, and the SAS controller at the same time, but the coordinated controller does not work (No-Coordinated Ctrl). The ESP controller, the SAS controller, and the coordinated controller (Coordinated Ctrl) are stimulated at the same time in the Fishhook test condition. The yaw moment and roll moment parameters of the coordination controller optimized by the

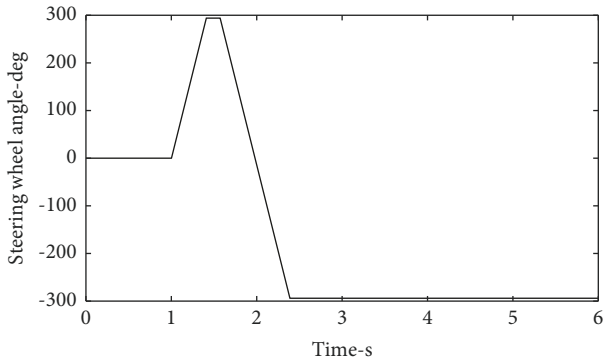

Figure 6: Fishhook test case diagram.

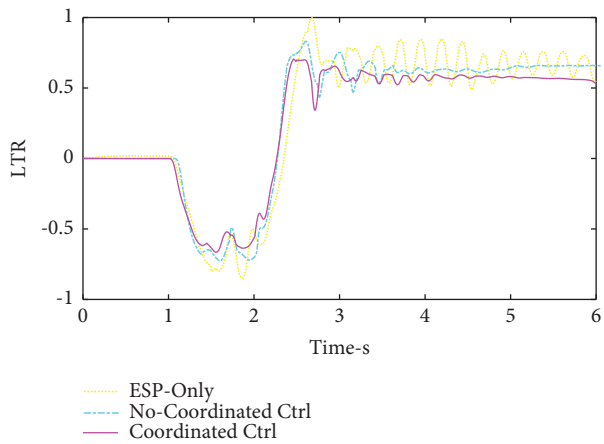

Figure 7: The variation curve of LTR with time.

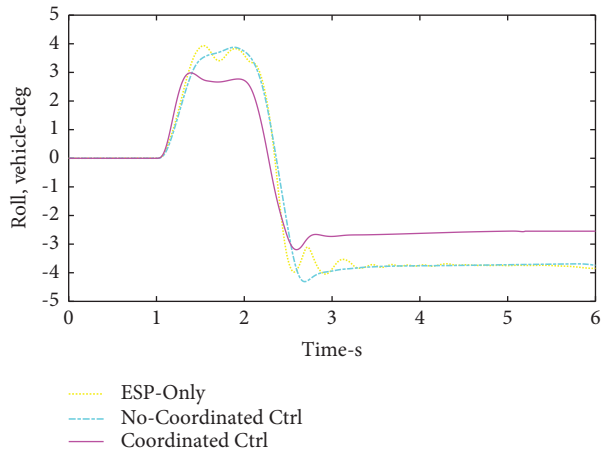

Figure 8: Variation curve of roll angle with time.

PSO algorithm are $k_1 = 8.4, k_2 = 7.2, k_3 = 9.4, k_4 = 4.8$. The simulation results are as follows.

It can be seen from Figure 7 that at 1.8 s, only the ESP-Only controlled test reached the critical value of LTR 0.8, and the LTR values of the No-Coordinated Ctrl and Coordinated Ctrl tests were less than 0.8; at 2.5 s, the LTR values for both ESP-Only and No-Coordinated Ctrl experiments reached the critical value of 0.8, with only the Coordinated Ctrl experiment having an LTR value of less than 0.8. The

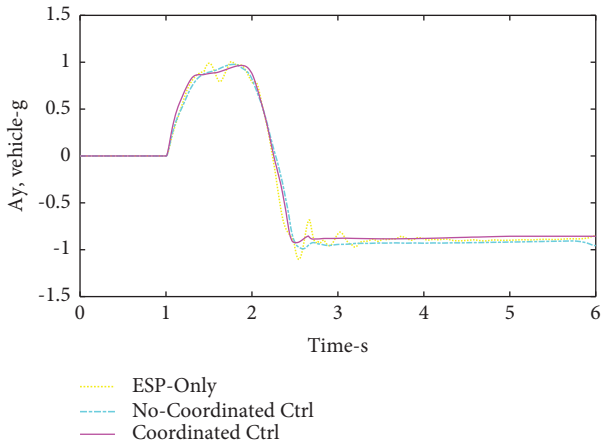

Figure 9: Curve of Ay versus time.

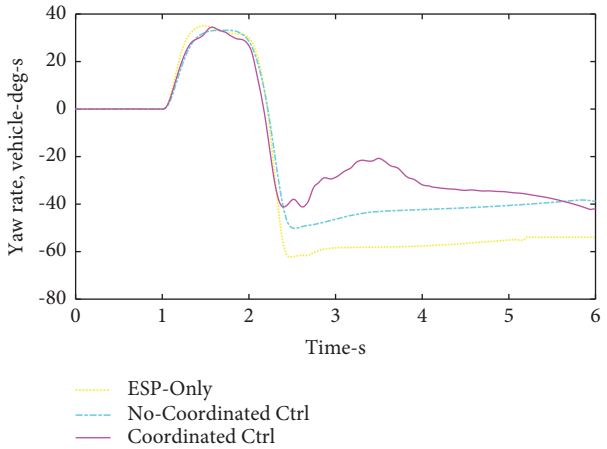

Figure 10: The curve of yaw rate with time.

result shows that in the whole Fishhook test, only the Coordinated Ctrl test did not have a rollover.

Among the above figures, Figures 8–10 are the curves of Roll angle, the lateral acceleration of the vehicle (Ay), and the Yaw rate with time, respectively. In the following table, Tables 1–3 are the relevant data of roll angle changing with time, Ay changing with time, and Yaw rate changing with time in the Fishhook test condition.

As can be seen from Figure 8 and Table 4, at 1.8 s, the roll angle of the vehicle with the coordinated controller is 20.83% lower than that of the vehicle without the coordinated controller, and 37.93% lower than that of the vehicle with ESP alone. After 3s, because the steering wheel angle of the vehicle is fixed, the roll angle of the vehicle without coordinated control is 2% higher than that of the vehicle with ESP alone, and the roll angle of the vehicle with coordinated control is 25% higher than that of the vehicle without the coordinated controller.

From the curve of Figure 9 and Table 5, the Ay of the vehicle with the coordinated controller is also improved compared with the Ay of the vehicle without the coordinated controller and the vehicle with ESP alone. It can be seen

Table 4: Table of roll angle changing with time in Fishhook test condition.

Times (s)	1	2	3	4	5	6
ESP-only (deg)	0.03	3.60	−3.94	−3.74	−3.72	−3.74
No-coordinated Ctrl (deg)	0.03	3.74	−3.93	−3.75	−3.74	−3.84
Coordinated Ctrl (deg)	0.04	2.71	−2.73	−2.62	−2.54	−2.54

Table 5: Table of Ay with time in Fishhook test condition.

Times (s)	1	2	3	4	5	6
ESP-only (g)	0.01	0.79	−0.94	−0.88	−0.89	−0.85
No-coordinated Ctrl (g)	0.02	0.82	−0.83	−0.93	−0.91	−0.95
Coordinated Ctrl (g)	0.02	0.87	−0.83	−0.87	−0.86	−0.84

Table 6: Table of yaw rate with time in Fishhook test condition.

Times (s)	1	2	3	4	5	6
ESP-only (deg/s)	0.01	30.1	−58.4	−57.3	−55.1	−53.9
No-coordinated Ctrl (deg/s)	0.01	28.5	−46.3	−42.2	−40.5	−38.8
Coordinated Ctrl (deg/s)	0.02	26.6	−28.7	−31.8	−34.9	−42.0

from Figure 10 and Table 6 that since the ESP controller is working during the whole test condition, the yaw rate of the vehicle in the three cases is the same before 2 s. After 2.5 s, the yaw rate of the vehicle with coordinated control is 50% higher than that of the vehicle controlled by ESP alone and 25% higher than that of the vehicle without coordinated control. Among them, the reason why the yaw rate of the vehicle with coordinated control fluctuates between 2.5 s and 4 s is that in this interval, the square plate in the direction of the vehicle is turning right 540 deg, and the value of LTR fluctuates.

From the above-given analysis, it can be seen that compared with the vehicle without the coordinated controller, the vehicle with the coordinated controller not only suppresses the overshoot and oscillation of the yaw rate and lateral acceleration but also significantly improves the roll and yaw of the vehicle and ensures the safe driving of the vehicle.

6. Conclusions

In this paper, the problem of improving the antiroll ability of the vehicle is studied. The ESP controller and the SAS controller are designed, respectively, and the coordinated control strategy is proposed based on the analysis of the coupling between ESP and SAS. The fuzzy control strategy and PID control strategy are used to design ESP controllers and SAS controllers, respectively. Simulations have been carried out to demonstrate the effectiveness of the proposed coordinated control system, of which the results show that compared with the ESP controller and noncoordinated controller, the proposed coordinated control strategy can effectively reduce the roll angle under roll conditions and has a good effect on vehicle roll control. However, there are also some influences of this paper: (1) the influence of vehicle pitch angle speed on vehicle yaw moment and roll moment is not considered; (2) without considering the operation in the actual algorithm, the accuracy and operation speed of the algorithm optimization parameters can be further improved. In response to these problems, we have planned future research work to improve the performance of yaw and roll coordinated control.

Data Availability

The labelled dataset used to support the findings of this study is available from the corresponding author upon request.

Conflicts of Interest

The author declares that there are no conflicts of interest.

Acknowledgments

The article was supported by Anhui Polytechnic University. This work was supported by the National Natural Science Foundation of China (NSFC) (Grant no. U21A20146), the Open Foundation Project of State Key Laboratory of Power System and Generation Equipment (Grant no. SKLD21KM09), the Synergy Innovation Program of Anhui Polytechnic University and Jiujiang District (Grant no. 2021cyxta2), and Wuhu Science and Technology Project (Grant no. 2021cg19).

References

[1] J. K. Li, Z. W. Li, W. W. Hua, and Z. H. W. Ni, "Statistical analysis of urban road traffic accidents," *Technology Innovation Application*, vol. 11, no. 21, pp. 74–76, 2021.

[2] R. Wei, Y. Li, C. Zhang, P. F. Li, and S. Su, "Research on casualty effects and characteristics of large and medium-sized bus in rollover major accident," in *Proceedings of the 14th China Intelligent Transportation Conference*, pp. 181–188, Springer, Singapore, May, 2019.

[3] S. Flügel, K. Veisten, L. I. Rizzi, J. de Dios Ortúzar, and R. Elvik, "A comparison of bus passengers' and car drivers' valuation of casualty risk reductions in their routes," *Accident Analysis & Prevention*, vol. 122, pp. 63–75, 2019.

[4] ZH. Y. Zhang, H. Feng, and W. W. Heng, "Accident analysis and influencing factors research on truck rollover," *Transport Energy Conservation & Environmental Protection*, vol. 17, no. 5, pp. 55–60, 2021.

[5] Y. J. Yang and X. M. Qiu, "The conditions and influencing factors of trucks' roll-over during turning," *Mechanics in Engineering*, vol. 41, no. 4, pp. 393–397, 2019.

[6] Ch. B. Sun, L. Fang, B. H. Tong, and J. D. Zheng, "Dynamic parameter sliding mode control of truck based on a T-S model," *Journal of Vibration and Shock*, vol. 40, no. 12, pp. 254–264, 2021.

[7] Q. F. Kong, Ch. J. Bao, Z. J. Jiao, and J. Wu, "Research on path tracking and anti-roll control of commercial vehicle based on takagi-sugeno fuzzy model," *IFAC-PapersOnLine*, vol. 54, no. 4, pp. 118–123, 2021.

[8] X. Li, X. Y. Xu, H. Zhang, and M. Y. Ma, "Mixed H2/H∞ tracking control for rollover prevention and yaw stability of commercial buses," *IEEE International Conference on Control and Automation*, vol. 6, pp. 1193–1198, 2020.

[9] J. P. Redondo, B. L. Boada, and V. Diaz, "LMI-based Hꝏ controller of vehicle roll stability control systems with input and output delays," *Sensors*, vol. 21, no. 23, p. 7850, 2021.

[10] C. H. B. Sun, L. Fang, and B. H. Tong, "Nonlinear robust fuzzy distributed control of vehicle steering with saturation constraint," *Journal of Vibration and Shock*, vol. 41, no. 4, pp. 77–85, 2022.

[11] Q. Q. Yao, Y. Tian, SH. Y. Wang, J. Q. Liu, and CH. Q. Wang, "Path traking control strategy intelligent vehicles based on force driv," *Journal of South China University of Technology*, vol. 50, no. 2, pp. 33–41, 2022.

[12] N. M. Negash and J. Yang, "Anticipation-based autonomous platoon control strategy with minimum parameter learning adaptive radial basis function neural network sliding mode control," *SAE International Journal of Vehicle Dynamics, Stability, and NVH*, vol. 6, no. 3, 2022.

[13] H. Y. Zheng, J. J. Wu, K. Q. Pan, W. J. Meng, and R. Li, "Research on control target of truck platoon based on maximizing fuel saving rate," *SAE International Journal of Vehicle Dynamics, Stability, and NVH*, vol. 4, no. 2, 2020.

[14] SH. Q. Li, P. Du, and X. Y. Feng, "Integrated anti-rollover control strategy of minibus," *Journal of Jiangsu University (Natural Science Edition)*, vol. 43, no. 2, pp. 131–138, 2022.

[15] J. W. Luo, P. S. Li, P. X. Li, and Q. Cai, "Observer-based multi-objective integrated control for vehicle lateral stability and active suspension design," *Journal of Sound and Vibration*, vol. 508, no. 9, pp. 116222–116225, 2021.

[16] S. Chen, H. D. Zhang, and H. D. Wu, "A research on vehicle rollover prevention based on combined control with active anti-roll bar and differential braking," *Automotive Engineering*, vol. 41, no. 9, pp. 1043–1049, 2019.

[17] Y. F. Zha, X. Y. Quan, F. W. Ma, G. Q. Liu, X. Zheng, and M. Yu, "Stability control for a four-wheel-independent-drive electric vehicle based on model predictive control," *SAE International Journal of Vehicle Dynamics, Stability, and NVH*, vol. 5, no. 2, 2021.

[18] F. J. Jia, H. H. Jing, Z. h. Y. Liu, and M. Q. Gu, "Cooperative control of yaw and roll motion for in-wheel motor vehicle with semi-active suspension," *Proceedings of the Institution of Mechanical Engineers - Part D: Journal of Automobile Engineering*, vol. 236, no. 1, pp. 3–15, 2022.

[19] E. Di Gialleonardo, A. Facchinetti, and S. Bruni, "Control of an integrated lateral and roll suspension for a high-speed railway vehicle," *Vehicle System Dynamics*, vol. 14, pp. 1–27, 2022.

[20] H. M. Qi, N. Zhang, Y. C. Chen, and B. H. Tan, "A comprehensive tune of coupled roll and lateral dynamics and parameter sensitivity study for a vehicle fitted with hydraulically interconnected suspension system," *Proceedings of the Institution of Mechanical Engineers - Part D: Journal of Automobile Engineering*, vol. 235, no. 1, pp. 143–161, 2021.

[21] T. Jayaraman, S. Palanisamy, and M. Thangaraj, "Hydraulic control valve integrated novel semi active roll resistant interconnected suspension with vertical and roll coordinated control scheme," *Journal of Automobile Engineering*, vol. 12, no. 7, p. 733, 2022.

[22] SH. Rahimi and M. Naraghi, "Design of an integrated control system to enhance vehicle roll and lateral dynamics," *Transactions of the Institute of Measurement and Control*, vol. 40, no. 5, pp. 1435–1446, 2018.

[23] S. Das, *Vehicle Dynamics Modelling: Lateral And Longitudinal*, pp. 407–412, Institute of Electrical and Electronics Engineers Inc, Noida, India, 2021.

[24] H. Termous, H. Shraim, R. Talj, C. Francis, and A. Charara, "Coordinated control strategies for active steering, differential braking and active suspension for vehicle stability, handling and safety improvement," *Vehicle System Dynamics*, vol. 57, no. 10, pp. 1494–1529, 2019.

[25] H. Q. Li, Y. Q. Zhao, F. Lin, and ZH. Xiao, "Integrated yaw and rollover control based on differential braking for off-road vehicles with mechanical elastic wheel," *Journal of Central South University*, vol. 26, no. 9, pp. 2354–2367, 2019.

[26] S. Chen, CH. G. Xia, SH. Y. Li, and X. Sun, "Study on the control of yaw and roll stability of the vehicle," *Journal of Machine Design*, vol. 35, no. 6, pp. 97–104, 2018.

[27] L. Yang and G. D. Zhang, "Research on body roll control Technology based on active lateral stabilizer," *Automobile Applied Technology*, vol. 15, pp. 53–55, 2020.